

Some new features of the passive scalar mixing in a turbulent flow

L. Danaïla, P. Le Gal, and F. Anselmet

I.R.P.H.E., U.M.R. 6594, Universités d'Aix-Marseille I & II, CNRS 12 Av. du Général Leclerc, 13003 Marseille, France

F. Plaza and J. F. Pinton

Laboratoire de Physique, CNRS U.M.R. 8514, E.N.S., 46 Allée d'Italie, 69364 Lyon, France

(Received 29 May 1998; accepted 30 November 1998)

We analyze experimentally the statistical properties of a turbulent mixing created in the gap between two counter-rotating disks at a Taylor Reynolds number $R_\lambda \approx 400$. Local isotropy is investigated for the inertial and dissipative scales r , using two tests, one applied on $C(r)$, the correlation coefficient between temperature increments and velocity increments, and the other one on $S(r)$, the temperature increment skewness factor. When heating one of the disks and cooling the other one, either positive, negative or almost null values of C and S can be obtained at small scales as a direct result of the presence of several temperature sources. In particular, we emphasize the fact that null or small values for these quantities in the inertial range are an evidence of local isotropy of the temperature field. In these cases, we use the Vaianti *et al.* equation [Physica D **73**, 99 (1994)] for the evolution of the temperature increments probability density functions (PDFs) to predict the inertial and dissipative range PDFs, using an initial PDF, and two measurable closure functions. The intermittent behavior quantified through these statistics is well reproduced by the numerical integration of this evolution equation. © 1999 American Institute of Physics. [S1070-6631(99)01703-1]

I. INTRODUCTION

Local isotropy of high Reynolds number turbulent velocity fields is a basic assumption of the universal similarity theory developed by Kolmogorov (K41). The K41 theory leads to the following scaling laws for the longitudinal velocity increments: $\langle (\Delta u)^p \rangle = \langle (u(r) - u(0))^p \rangle \approx \bar{\epsilon}^{p/3} r^{p/3}$, when r lies in the inertial range, and where $\bar{\epsilon}$ is the mean dissipation rate.¹ These moments are characteristic of self-similar probability density functions (PDFs). However, experimental studies report significant deviations of the high order velocity² moments from these universal statistics and this behavior is classically attributed to the internal intermittency of turbulence. Consequently, an important small-scale property of high and moderate Reynolds number turbulence is the level of internal intermittency, i.e., the spatial localization of the “fine structures” of turbulence responsible for the fluctuations of the kinetic energy dissipation rate. A quantitative measure of this phenomenon is obtained from the study of the PDFs associated with the inertial and dissipative scales, which are non Gaussian, but possess exponential tails.

It was then reasonable to believe that details of the structure of the scalar field advected by a fully turbulent flow would follow automatically from a better understanding of the velocity properties and that the K41 theory could be extended to the description of the scalar fields mixed by turbulence.³ The result is the Kolmogorov-Obukhov-Corrsin—hereafter referred to as KOC—scaling theory. But it appeared⁴ that, the intermittent nature of energy transfer from large to small scales is for scalars more complex than expected,⁵ and various statistical approaches have been developed over the last years to analyze theoretically the

anomalous scaling exponents of the temperature structure functions $S_{2n}(r) = \langle (\theta(r) - \theta(0))^{2n} \rangle$.⁶⁻⁹ In particular, an original approach has been developed in Ref. 10, permitting us to obtain the temperature increment PDF evolution through the scales, starting from initial statistics at a particular scale and using two conditional expectations which can be measured¹¹ or computed.¹² Let us remark that all of these different theoretical approaches need, as a starting point, the local isotropy of the passive scalar mixing, which is in fact never totally experimentally respected. For instance, as the Vaianti *et al.* theory supposes null odd moments associated with symmetric PDFs and closure functions, it has been emphasized¹² that the PDF equation is verified only for the range of scales where the local isotropy of the mixing is respected. This range covers the small scales and extends up to a maximum scale that depends on the Péclet number and the large-scale mean temperature gradient.¹² Some of the experimental data were even symmetrized, in order to force the odd moments to zero, and to simulate the behavior of a perfectly isotropic field. In fact, many studies over the last decades have also revealed that the scalar field exhibits more anomalies than the velocity field, and that the scalar proves to be a very sensitive detector revealing subtle aspects of turbulence itself. In particular, one of these most striking anomalies in the shear flows lies in the observation that the scalar longitudinal derivative skewness factor significantly departs from zero.¹³⁻¹⁸ This phenomenon, usually attributed to the formation of ramps¹³ or cliffs¹⁷ which localize the temperature gradients on more or less two-dimensional regions of the flows, consequently invalidates the isotropy hypothesis.

In the present study, we investigate the possibility to

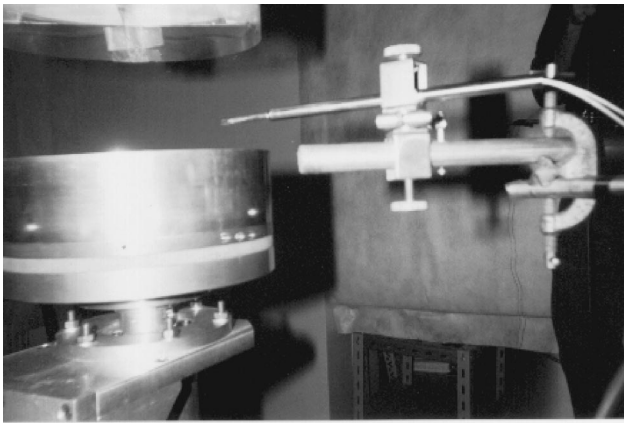


FIG. 1. Experimental set-up.

experimentally create a substantial level of isotropy of the mixing of a passive scalar, and we verify several tests and consequences associated with this feature. We will first present, in Sec. II, the experimental set-up and the flow characteristics. In Sec. III, we will then show that isotropy can be obtained for the temperature field, when there exists a range of scales for which the following two conditions are satisfied: null velocity-temperature increment correlation coefficients, and zero temperature increment skewness factors. As mentioned before, these properties are quite original and have been obtained by the association of a cold and a hot source applied on a room temperature flow. It was also reported in the past that asymmetrical heating could give some unusual properties, due to the creation of a counter-gradient turbulent heat diffusion.^{19,20} For the case of the present study, we will emphasize some other characteristics such as symmetric temperature increment PDFs and symmetric conditional expectations. Finally, in Sec. IV, we will verify that the temperature increment PDFs evolution, computed by the integration through the scales of the Vainenti *et al.* equation, is in fair accord with the measured PDFs for the scales smaller than 80η (where η is the Kolmogorov length scale).

II. EXPERIMENTAL SET-UP

We study the mixing created in the gap between two counter-rotating disks, in air. This set-up, represented in Fig. 1, is known to produce a strong intensity turbulence in a compact region of space.^{21,22} More details about this experimental set-up can be found in Refs. 22,23. The disks have a radius $R=10$ cm, and they are separated by a distance $H=22$ cm. In order to increase the entrained fluid quantity, they are equipped by a set of 8 vertical blades (thickness 5 mm, height 20 mm) and by two skirts (height $h_s=55$ mm). The rotation axis is vertical.

Temperature fluctuations are created by cooling the upper disk and heating the other one with respect to the ambient temperature (24°C). This is an original means to create mean temperature gradients, in the sense that, traditionally, only a single heat source is used (for instance in a heated boundary layer or a heated jet). We will see later on that the

presence of these two sources, associated with the particularities of this swirling flow, does lead to an original scalar field behavior.

More specifically, the lower disk is made of copper and it is heated by a classical electrical resistance. The surface temperature on the heated disk can be imposed, and it is about 35°C . The upper disk is made in aluminum and it possesses a hollow cavity where dry ice may be placed. In these conditions, when the disks are spun, a stationary state can be reached, and the surface of the upper disk keeps a constant and uniform temperature (-5°C) for runs of about 10 min duration. So, the surface temperature varies from 35°C on the bottom, to -5°C on the top disk. On the other hand, thin thermal boundary layers develop on the surface of each disk, where the mean temperature profiles present steep gradients. Therefore, in the central zone, which extends on about 11 cm (approximately $H-2h_s$, see Fig. 1), the maximum mean temperature difference between its top and bottom, is 4°C . Hereafter, only this measurement zone will be investigated.

In all experiments, the thermal field is passive, i.e., the statistical characteristics of the velocity field are the same as those in the non-heated-flow. In order to study the phenomenon that governs the transfer through the scales of the temperature variance, we have to explicitly take into account the velocity role. Therefore, simultaneous temperature-velocity measurements are performed using a dual probe which includes a cold wire and a hot wire. These wires are parallel and distanced by 0.4 mm.

We use a $5\ \mu\text{m}$ diameter hot wire, with an active length of 1 mm, resulting in a length to diameter ratio of approximately 200. It is operated by a TSI IFA 100 constant temperature anemometer with an over-heat ratio of 1.6.

The cold wire has a $0.6\ \mu\text{m}$ diameter d , a total length of 2 mm and an active etched length l of 0.5 mm, so that the ratio l/d is about 800. This value is an optimum, resulting from two criteria: (1) Heat conduction between the etched region and the stubs or prongs is a significant source of errors, for cold wire lengths $l/d \leq 1000$.²⁴ Unfortunately, larger values would lead to the violation of the second criterion. (2) The spatial resolution of the wire. This is a special requirement in order to correctly determine small-scale characteristics such as derivatives or increments. The spatial resolution corrections for the cold wire could be made using the method described in Ref. 25, for spectra or the temperature mean dissipation rate. Typically, in our measurements, the active length is $l \approx 4\eta \approx (4/1.28)\eta_\theta = 3.12\eta_\theta$. Note that, for such a length, the scalar dissipation is underestimated.²⁵

Therefore, we consider that the chosen length is a good compromise between these criteria, and we will discuss later on the possible limitations of our results. Note that similar end-effect problems are met for the hot-wire for which l/d should be larger than 200, which is just the value we use.

The cold wire is operated by a constant current circuit with the sensitivity $0.1\ \text{mV}/^\circ\text{C}$, at a very low overheat ratio (current 0.1 mA) to minimize contamination by velocity. Also, in order to avoid the contamination of the cold-wire measurements by the hot wire wake, the probe is placed in a region of the flow where a mean stream exists, near the disk

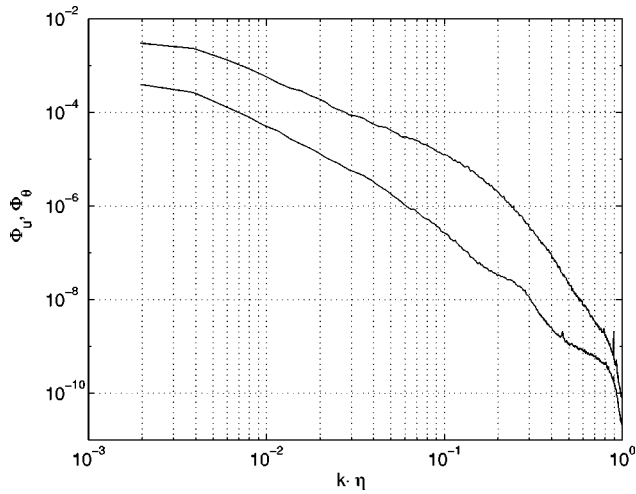


FIG. 2. Typical spectra for temperature (lower curve) and velocity (upper curve).

periphery, and the cold wire is positioned upstream. Note that the velocity has an azimuthal and a radial component. In the central zone, we mainly measure this radial component. The effect of the temperature fluctuations on the hot-wire measurements has been determined to be less than 1% using the method presented in Refs. 26,27. This small difference reported here is explained by the fact that most of the measurements have been made in the central part of the experimental set-up, where mean temperature differences with respect to the ambient are about 0.5 °C only. This effect is not corrected.

Data are digitized at a frequency of 78125 Hz, with a resolution of 23 bits and stored using a VXI Hewlett-Packard E1430 digitizer. All records include at least 10^6 points.

III. SOME ISOTROPIC PROPERTIES OF MIXING

A. Temperature and velocity spectra

Let us first present a brief summary of the flow conditions. We study a double sheared flow, produced by the counter-rotating regime of the disks. The rotation frequency Ω of the disks is variable, between 20 and 40 Hz. The integral scale Reynolds number is $Re = R^2\Omega/\nu \approx 10^5$, and the turbulent Reynolds number is typically $R_\lambda \approx 400$, but the largest value we obtained is as large as 600, corresponding to a fully developed turbulent flow. The total velocity fluctuation RMS is $u' \approx 3$ m/s, and the mean total velocity at the position the sensor is placed, is between 7 m/s and 12 m/s, depending on the rotation regime. The typical temperature RMS lie between 0.1 °C and 0.15 °C. The Kolmogorov scale is in the range 50 μm –80 μm , and the Taylor micro-scale for the dynamic field λ is in the range 1 mm–2.5 mm. Both scales were classically estimated using the isotropic approximation for $\bar{\epsilon}$, the velocity mean dissipation rate, inferred from the integration of the velocity derivative spectrum.²⁸

Figure 2 shows typical spectra for velocity and temperature (shifted downwards), using usual ordinates. The Reynolds and Péclet numbers of the experiments corresponding

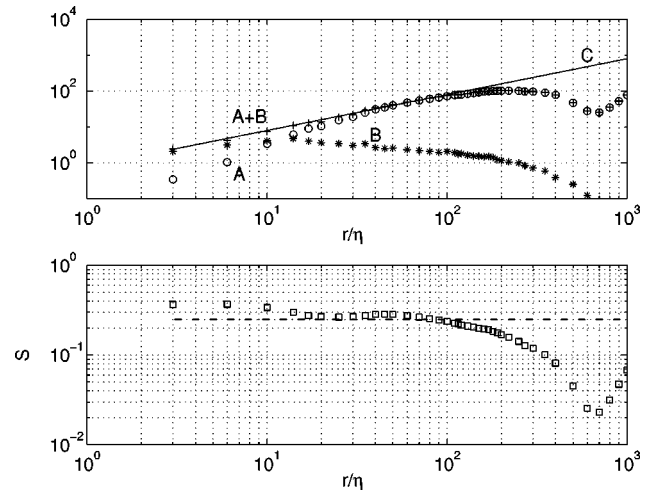


FIG. 3. Third order velocity structure functions as a criterion to define the inertial range. (a) Kolmogorov's equation verification: term A (\circ) and term B ($*$). A+B ($+$) to be compared with C (solid line). (b) Velocity increments skewness factor (\square). The dashed line is 0.25.

to these plots are $R_\lambda = 600$ and $Pe_\lambda \approx 400$. The intermittent behavior is particularly visible on the temperature spectrum, whose slope is slightly lower than $-5/3$.¹⁵

A classical way to observe the inertial range is to study the velocity structure functions.

Figure 3(a) presents the balance between the three terms of Kolmogorov's equation,

$$\langle(\Delta u)^3\rangle - 6\nu \frac{d}{dr} \langle(\Delta u)^2\rangle = -\frac{4}{5} \bar{\epsilon} r, \quad (1)$$

written in the dimensionless form,

$$-\langle(\Delta u)^3\rangle/(\bar{\epsilon}\eta) + 6\nu \frac{d}{dr^*} \langle(\Delta u)^2\rangle/(\bar{\epsilon}\eta^2) = \frac{4}{5} r^*,$$

where $r^* = r/\eta$. The scales r are calculated using Taylor's hypothesis using the mean velocity. More details about the behavior of the moments of the scalar are given in Ref. 23. The turbulent transport term $A = -\langle(\Delta u)^3\rangle$ presents a linear behavior in the inertial range equalizing the total-dissipation term $C = \frac{4}{5} \bar{\epsilon} r$, and it equilibrates the dissipative term B at about 15η . This is the upper limit of the dissipative range. Remark here that the mean dissipative rate was computed using the assumption of isotropy for the dissipative scales, $\bar{\epsilon} = 15\nu \langle(\partial u/\partial x)^2\rangle$.

Alternatively, the dissipative rate is computed using the isotropic relation, $\bar{\epsilon} = 15\nu \int_0^\infty k_1^2 \Phi_u(k_1) dk_1$, where $k_1 = 2\pi f/U$ is the wave number, f is the frequency in Hz, and U is the mean velocity. A quite good agreement between these two methods is obtained.

The Kolmogorov equation verification, see Fig. 3(a), clearly emphasizes that, at this large R_λ number, the typical inertial range is between 20η and 150η .

One may also define the inertial range from the properties of the third-order structure function skewness factor, $-S = \langle(\Delta u)^3\rangle/(\langle(\Delta u)^2\rangle)^{3/2}$, which should present a 0.25 plateau in the inertial zone,¹¹ when both moments obey the

Kolmogorov scaling law. Figure 3(b) shows that a plateau at 0.25 is indeed reasonably well defined in the inertial range.

Both tests are well-satisfied at this large Reynolds number, and they are not sensitive to the intermittency effects.

B. Velocity-temperature correlations

Examining the correlation coefficients between velocity and temperature increments,

$$C(r) = \langle \Delta u \Delta \theta \rangle / \sqrt{\langle (\Delta u)^2 \rangle \langle (\Delta \theta)^2 \rangle},$$

provides a particularly interesting point of view to study the transfer from the large to the small scales. Indeed, the sign of C at large scales is characteristic of the way temperature fluctuations are generated, whereas a null correlation at small scales is an indicator of isotropy for the temperature field. Explicitly, the more rapidly these correlations C become null, the faster the isotropic stage is attained. Note that the value of C tends to the velocity-temperature correlation coefficient for very large separations r .

In our experiments, the double nature of the source of temperature fluctuations allowed us to obtain three regions in the flow:

- (1) The first one, near the hot disk, where velocity-temperature correlations are positive. Warm air moves rapidly, and the flow behaves similarly to a heated jet.
- (2) The second one, near the cold disk, where the velocity-temperature correlations are negative. Cold air is fast, and the flow behaves as a heated turbulent boundary layer.
- (3) A central region, where these correlations are almost null, obviously much smaller than the correlations measured nearer the disks. Concretely, we consider that this correlation coefficient is null, when $|C(r)| \leq 0.05$ in the inertial zone. For the large injection scales, it is obvious that $C(r)$ will take the sign of the disk having the stronger influence. Let us note that this central region is known to preserve the homogeneity and the isotropy of the velocity field.^{21,22}

The three regions are referred to as F_+ , F_- , and F_0 , differing by the position of the sensor or by the mean velocity gradient applied between the disks.

As the rotation frequency of each disk is variable, the mean total velocity at the periphery of the disks may also differ, from one run to another. Let us call them Ω_c for the cold disk, and Ω_h for the hot disk, so the periphery mean azimuthal velocities are $V_c = 2\pi R\Omega_c$ and $V_h = 2\pi R\Omega_h$, respectively. The mean azimuthal velocity profile varies between $+V_h$ to $-V_c$ over a distance H . Approximatively, the mean radial azimuthal velocity will be zero at a position $H_0 = V_h / (V_h + V_c)H$. At this position, the mean velocity is then maximum by incompressibility. This benchmark will be further used in order to position different measurements; a position h^- signifies that the measurement is performed above the point H_0 , on the side of the cold disk, a position h^+ is near the hot disk.

We illustrate these three types of correlation coefficients in Fig. 4 which emphasizes in particular the large range of

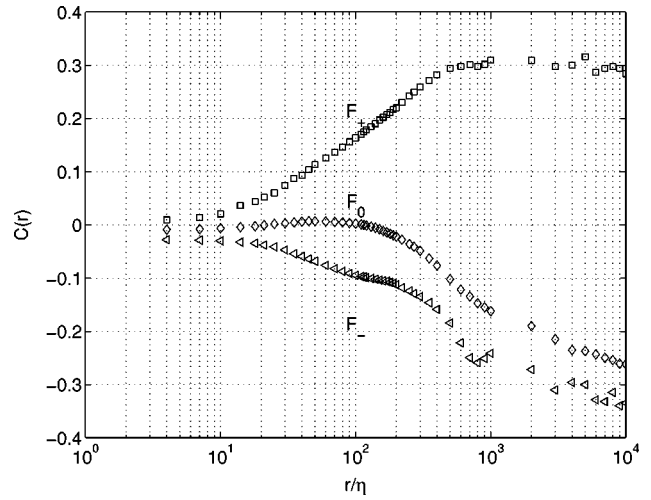


FIG. 4. Correlation coefficients $C(r)$ between velocity and temperature increments: measurement in F_+ region (\square , $h^+ = +2.5$ cm), measurement in F_0 region (\diamond , $h^- = -5$ cm), and measurement in F_- region (Δ , $h^- = -8.5$ cm).

correlation coefficients that can be obtained, thus illustrating the wide variety of mixing properties available in our flow configuration. For this set of measurements, the mean temperature in the hot side of the measurable zone is 28 °C, in the cold side it is 24 °C, and the ambient temperature is 24.5 °C.

However, as it can be seen in Fig. 4, all these situations display correlation coefficients that go to zero at very small scales. This feature was also found in previous ‘‘classical’’ experiments¹¹ and it is in very good agreement with local isotropy. Note for instance that this test was used to check the measurement quality in a heated boundary layer by Ould-Rouis *et al.*¹¹

Taking into account the fact that the integral scale L is about 1200η , (computed as $L/\eta \approx (R_L)^{3/4} = (R_\lambda^2/15)^{3/4}$), and the inertial range extends between scales smaller than 150η , and larger than about 20η , we thus succeeded in obtaining a correlation coefficient null through all the inertial range in the F_0 case. To our knowledge, this is the first time that such a verification of the scalar isotropy property is found, at least over such a large range of scales.

Let us remark here that the correlation coefficient $C(r)$ is a physical magnitude linking statistically the temperature variations, with the velocity variations. We propose further a second test of isotropy, concerning the passive scalar scalar itself: the symmetry coefficient of the temperature increments.

C. Temperature increment skewness factors

As a second step, we will now analyze measurements in the central region (F_0), which satisfy the isotropy requirement for a wide range of scales from the correlation coefficient point of view. We submit these experimental data to another isotropy test, by studying the temperature increment skewness factor, $S(r) = \langle (\Delta \theta)^3 \rangle / \langle (\Delta \theta)^2 \rangle^{3/2}$. By isotropy, this quantity has to be null for sufficiently small scales. In the literature, it is classically found that the temperature in-

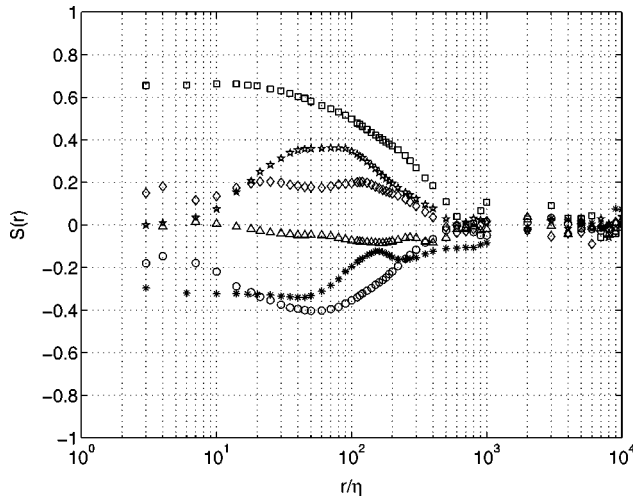


FIG. 5. Temperature increment skewness factors $S(r)$ for various F_0 cases, from upper to bottom side: $h^- = -9$ cm (\square), $h^- = -8.5$ cm (\star), $h^- = -7$ cm (\diamond), $h^- = -1.5$ cm (\triangle), $h^+ = +0.5$ cm (\ast) and $h^+ = +2.6$ cm (\circ).

crement skewness factor computed along different flow directions does not tend to zero, but remains constant, as a sign of the small-scale persistent temperature anisotropy.^{13–15,17,29} Usually, this constitutes a strong argument for the small-scale residual anisotropy and specific studies have been carried out to determine the factors which lead to nonzero temperature increment skewness factors. Two directions have been more specifically followed:

- Considering shearless flows is the first approximation permitting to simplify the reality. This has led to the conclusion that in numerical studies without shear, or in grid turbulence, the mean temperature gradient is the main factor responsible for the residual temperature derivative skewness factor, in the direction parallel to the mean temperature gradient.^{17,29} In the direction perpendicular to this large-scale anisotropy, the skewness factor is effectively zero.
- However, shear flows correspond to the most realistic situation, and it has been concluded that the temperature derivative skewness factor also exists in the direction perpendicular to the mean temperature gradient, as a direct effect of the combination of the local shear, and the mean temperature gradient.^{13–15}

We will show here that it is nevertheless possible to obtain a quasi-null skewness factor, as an intermediate state between positive and negative skewness factors. As Fig. 5 shows, even if these measurements are characterized by a very small correlation coefficient $C(r)$, a large variety of skewness factors is obtained. The skewness factors depend on the scale r/η , but also on the different measurement positions in the central region between the disks. The succession of curves presented in this figure is obtained when moving the probe in the central region, from the cold disk (upper curves) towards the hot disk (lower curves), along a physical distance of 6 cm, situated in the center part of the measurable zone. We recall that the position h^+ or h^- is not character-

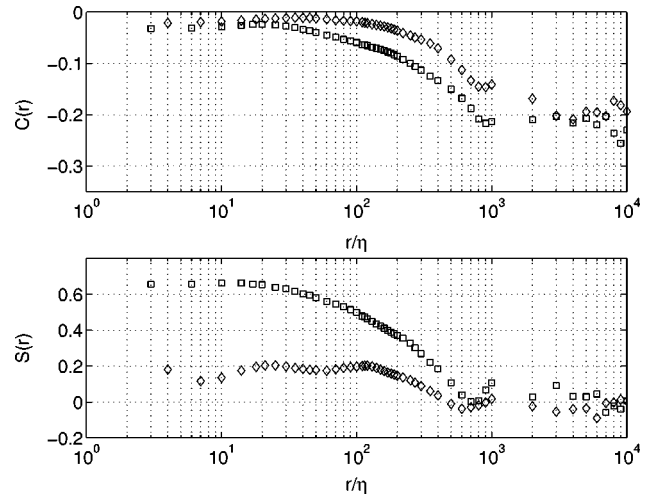


FIG. 6. Comparison between $C(r)$ (top) and $S(r)$ (bottom) for two different sets of measurements in the F_0 cases: at $h^- = -9$ cm (\square) and $h^- = -7$ cm (\diamond).

istic of the geometrical position, but of the “regime position,” which takes into account the disk rotation frequency.

Temperature increment skewness factors usually present a plateau as the scale goes to zero, as it should arise from KOC scaling laws. Therefore, a $S(r)$ plateau obtained for the scales $r \leq 10\eta$ (as it is the case here), is a good verification of the measurement quality. On the other hand, if the KOC theory is to be valid, isotropy imposes that all of these odd order moments should be zero. This is a strange behavior of the skewness factors, which is worth being understood.³⁰

At the large injection scales, $S(r)$ is always zero, by homogeneity and no-correlation between temperature fields $\theta(x)$ and $\theta(x+r)$. Figure 5 provides a good indication about the integral scales (larger than 1000η), where all skewness factor curves go to zero, which is in good agreement with the value of about 1200η we have reported in the previous subsection.

For the smaller scales, $S(r)$ evolves together with the correlation-coefficient $C(r)$, as it can be seen in Fig. 6: a variation on the correlation coefficient implies a variation on the skewness factor. In particular, when $C(r)$ is equal to zero, so that local isotropy is reached, the $S(r)$ evolution is frozen till the small dissipative scales. This observation means that the scalar environment, i.e., the dynamic field, here represented by the correlation coefficient $C(r)$, is responsible for the possible isotropic conditions for the temperature field.

A possible way to learn more about the temperature increment skewness factors would be to study an equation through the scales for this quantity. In particular, in Ref. 31, an equation for the temperature derivative skewness factor was obtained in a shear flow, but the balance between all terms is rather difficult to verify.

In fact, the positive skewness factors correspond to the measurements performed in the cold part of the central zone. This means that the rare and strong velocity fluctuations are preferably associated with cold pockets of fluid, and this is persistent even for the small scales. The temperature incre-

ment skewness factor has the same sign as the temperature derivative skewness factor. Thus, the positive sign of S near the cold disk is in perfect agreement with the theoretical sign obtained for the temperature derivative skewness factor in Ref. 31. This sign was obtained taking into account the mean temperature gradient sign and the shear sign.

Similarly, a negative skewness factor is obtained in the hot part of the central zone, where the mean temperature gradient keeps its sign, but the shear sign is opposite, since the radial component of velocity presents a maximum at H_0 . The two temperature sources are indeed necessary in order to maintain temperature fluctuations across the whole flow. Between these zones, it is therefore possible to obtain nearly zero increment skewness factors, as it can be seen in Fig. 5. This state is a transitory state between two states associated with opposite signs. In a way, a zero skewness factor is created in our flow configuration as an inevitable state between two kinds of mixing. A large range of values has also been obtained for the derivative skewness factor (computed by the increment at the scale 2η), which varies from -0.6 to $+0.8$. In particular, as we have just emphasized, a null temperature derivative skewness factor can be achieved contrary to what is usually obtained in a shear flow with a single-temperature source mixing, where a large value for the derivative skewness factor is reported (approximately 0.8 in modulus).³¹ However, note that in the case of heated grid turbulence, the magnitude of the temperature derivative skewness factor which is small (≈ -0.3) has also been reduced to zero (≤ 0.05) by perturbing the flow with a second grid at ambient temperature.³²

In fact, the same features can be observed on the temperature field itself which presents a large variation in the skewness factor which goes from values around 1 near the heated disk, to -1 near the cold disk. Nevertheless, we could not so far establish a quantitative linkage between the small-scale value of $S(\Delta\theta)$ and $S(\theta)$, since an obvious coupling with the velocity field is also to be taken into account. In particular, it is worth recalling that in a "classical flow" such as a heated jet or a heated boundary layer, ramps have opposite signs, and this sign is always the same for each of these flows, regardless of the measurement station in any of these flows. However, in any given particular flow, the temperature skewness factor may take different values of both signs. For instance, in a heated boundary layer, $S(\theta)$ varies from about -0.3 in the heated wall region, whereas it is about $+0.5$ in the outer region (with even larger positive values closer to the interface region).

As already discussed in the introduction, a simple physical image of the temperature field, permitting in a way to explain these non zero skewness factors, is the ramp model of temperature^{13,33} where the direction of the ramps is given by the temperature mean gradient sign multiplied by the shear sign. Figure 7(a) presents a temperature signal close to the heated disk, where temperature ramps are well defined, and the skewness factor of the temperature signal is equal to -0.6 , while the temperature derivative skewness factor is 0.32. Figure 7(b) shows a temperature signal in a case of symmetric mixing, where ramps are observed in both directions. The temperature skewness factor is greatly decreased

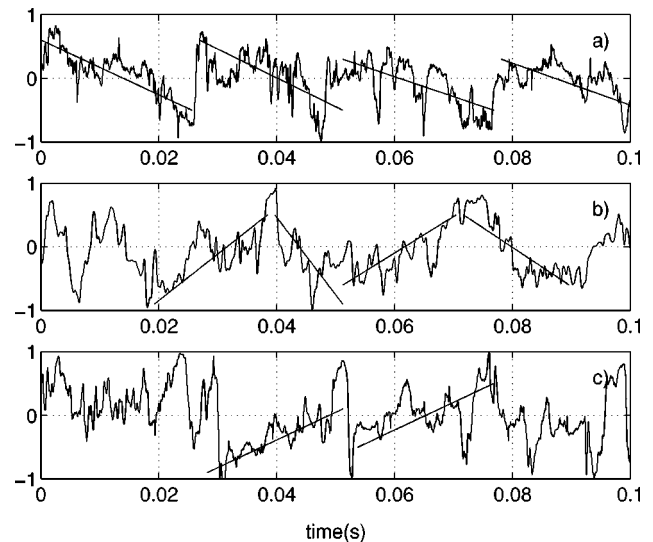


FIG. 7. Temperature signals for three kinds of mixing, using arbitrary units. (a) Near the hot disk $h^+ = +2$ cm, (b) in the central zone $h^- = -3$ cm, (c) near the cold disk $h^- = -8$ cm.

in this case and takes a value near 0.1. The temperature derivative skewness factor is 0.08 for this case. Finally, Fig. 7(c) shows a signal recorded near the cold disk where ramps can also be observed. In this case, the temperature skewness factor is about $+0.5$. The time period presented in these three plots corresponds approximately to 4 rotations of the disks (the rotation frequency is 40 Hz), and a ramplike structure approximately appears at each rotation period. In the central part of the mixing, the cold ramps meet the hot ramps, and they can cancel one another on average and create a symmetric stage, so that a quasi-isotropic mixing can be obtained statistically.

Thus, a sheared mixing having a double temperature source can produce, in a central region, a quasi-isotropic zone, where the temperature increment skewness factors are very small, and the temperature derivative skewness factor is much smaller than what is usually obtained. All these efforts which are necessary to obtain a quasi-null longitudinal derivative skewness factor, in a region where velocity-temperature increment correlation coefficients $C(r)$ are small, demonstrate that the local isotropy property of the passive scalar field is not at all an obvious natural state in shear flows with a mean temperature gradient. However, our measurements prove that an almost perfectly isotropic state is possible in this particular heated and cooled shear flow. In fact, our flow configuration permits to mix a cold turbulent flow created by the cold disk and a warm turbulent flow created by the warm disk. The verification of the local isotropy property will now permit to investigate more deeply the characteristics of the scalar field and in particular its intermittent behavior.

IV. PREDICTION OF THE EVOLUTION THROUGH THE SCALES OF THE TEMPERATURE INCREMENT PDFS

A. The PDF equation and the closure problem

In the previous section, we have examined the mixing symmetry, as an isotropy test in the direction normal to the

mean temperature gradient. As the real isotropy (rotational invariance) cannot be directly tested in experiments, different methods are proposed in the literature: if isotropy exists, exact theoretical results may be deduced related to different levels of approximation. These relations are then submitted to verification (relations between lateral and longitudinal spectra, even-order structure functions, odd-order structure functions, etc.). As a consequence, when a conclusion about isotropy is pointed out, it is always related to a specific criterion.³⁴

In what follows, the properties of our quasi-isotropic mixing will be further analyzed and used to predict the evolution through the scales of the temperature increment PDFs.

More specifically, the isotropy properties described in the preceding paragraphs, null velocity-temperature correlations and very small temperature increment skewness, will be used to solve numerically the evolution equation obtained by Vaienti *et al.*:¹⁰

$$\begin{aligned} & \left[\frac{2}{r} + \frac{\partial}{\partial r} \right] [P(r, X) q_1(r, X)] + 2k_0 \frac{\partial^2}{\partial X^2} [P(r, X) q_2(r, X)] \\ & = 2k_0 \left[\frac{2}{r} + \frac{\partial}{\partial r} \right] \frac{\partial P}{\partial r}(r, X), \end{aligned} \quad (2)$$

where k_0 is the molecular diffusivity coefficient, $X = \Delta \theta(r) = \theta(x+r) - \theta(x)$, and $P(r, X)$ is the probability density function of the temperature increment X , at the scale r . This equation was derived using the assumptions of homogeneity and three-dimensional isotropy of the temperature fluctuations. One of the main constraints was therefore that all temperature increment odd-order moments be strictly equal to zero or, equivalently, that all PDFs be perfectly symmetric. The closure problem then consists in determining two conditional expectations: that of the longitudinal velocity increments conditioned by the temperature increments, $q_1(r, X) = \langle \Delta u | \Delta \theta \rangle$, and that of the square temperature gradient conditioned by the temperature increments, $q_2(r, X) = \langle (\nabla \theta)^2 | \Delta \theta \rangle$, where $\nabla \theta$ is evaluated at location x , using a finite difference scheme with the smallest separation 4η . Figure 8 presents these conditional expectations, for different scales, as a function of dimensionless temperature increments: X/θ' , where θ' is the temperature RMS.

These conditional expectations have been previously determined experimentally for a boundary layer over a heated wall¹¹ and for a direct numerical simulation.^{29,12} To simulate isotropy, the Eq. (2) verification then needed symmetrization of the PDFs and both conditional expectations.¹² In the present case, the very small temperature increment skewness factors explicitly lead to almost symmetric PDFs for the entire inertial range. Also, the conditional expectation q_1 is almost symmetric [see Fig. 8(a)] for the scales smaller than 120η , contrary to its evolution in the boundary layer turbulence.¹¹ In particular, its typical ‘‘A’’ shape¹¹ is reasonably well recovered in almost the whole inertial zone, despite oscillations of non negligible amplitude. Determining q_1 with great accuracy is a very difficult task since the variances of both Δu and $\Delta \theta$ are strongly reduced when the scale r gets smaller and smaller. Moreover, it can be observed that

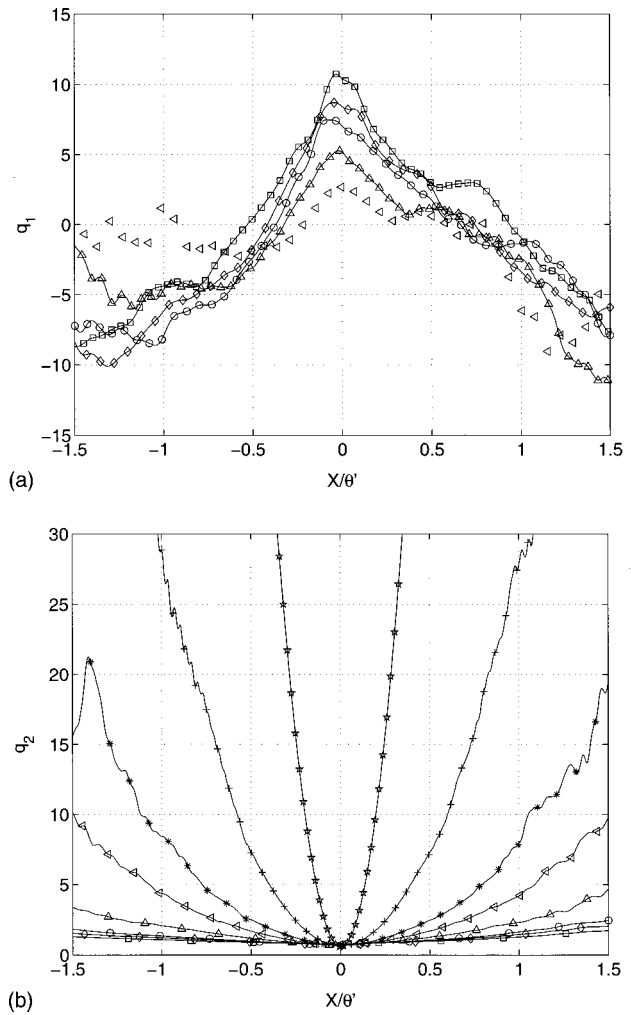


FIG. 8. Conditional expectations q_1 (a) and q_2 (b), function of temperature increments rendered dimensionless using the temperature RMS θ' , for the symmetric mixing situation. For both figures, different scales are represented using the same symbols: 120η (\square), 80η (\diamond), 60η (\circ), 30η (\triangle), 15η (∇). For the conditional expectation q_2 , additional scales are represented: 10η ($*$), 5η ($+$), and 2η (\star), in order to emphasize the small-scale trend of q_2 .

its scale evolution is quite weak, according to the fact that this conditional expectation q_1 is related to the stationary state of the velocity-temperature increment correlation coefficient. To compute the q_2 conditional expectation, isotropic approximations have been used (i.e., three times the temperature square longitudinal derivative). As it was the case in Ref. 11, q_2 evolves from an horizontal line at large scales to a parabola at small scales [see Fig. 8(b)]. Note that only a selected subset of the data points has been plotted using symbols in Fig. 8, in order to prevent clutter.

Finally, let us remark the parallel between our approach, which needs two closure information, and the study of the ‘‘balance equation.’’⁸ Indeed, our first closure function lies on a measurement of the velocity field (q_1 function), whereas the closure of the theoretical problem presented in Ref. 8 supposes that the velocity field is Gaussian and delta correlated in time. Also, our second closure (the measurement of the q_2 function) concerns the dissipation field, as it is the case in the ‘‘linear ansatz’’ considered in Refs. 8,9.

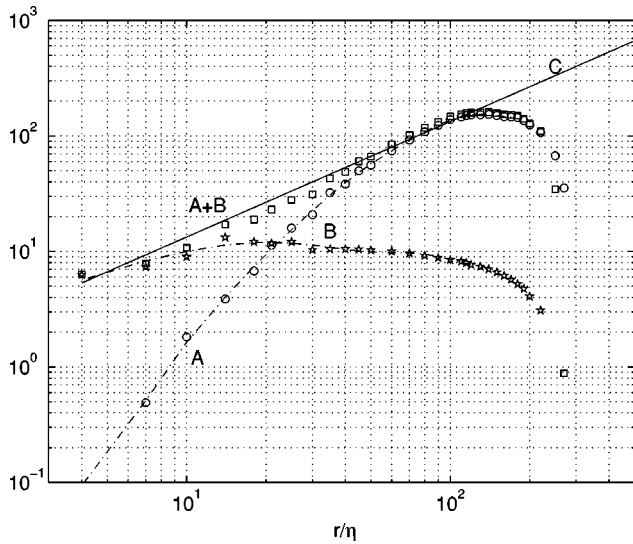


FIG. 9. Yaglom's equation verification: advective term A (\circ) equilibrates dissipative term B (\star) at 20η . $A+B$ (\square) balances C (solid line), for the scales smaller than 150η .

B. Yaglom's equation

Let us remark that Yaglom's equation,³⁵

$$-\langle \Delta u (\Delta \theta)^2 \rangle + 2k_0 \frac{d}{dr} \langle (\Delta \theta)^2 \rangle = \frac{4}{3} k_0 \langle (\nabla \theta)^2 \rangle r \quad (3)$$

is a particular case, at the second order, of Eq. (2). In particular, each term of 3 can be rewritten using the two conditional expectations q_1 and, in an implicit form, q_2 :

$$\begin{aligned} & - \int_{-\infty}^{+\infty} q_1(r, X) \cdot X^2 \cdot P(r, X) dX + 2k_0 \frac{d}{dr} \int_{-\infty}^{+\infty} X^2 \cdot P(r, X) dX \\ & = \frac{4}{3} k_0 \langle (\nabla \theta)^2 \rangle r. \end{aligned} \quad (4)$$

However, it is worth emphasizing that Yaglom's equation [as well as its velocity counterpart, Kolmogorov's Eq. (1)] is not sensitive to small scale intermittency since it only characterizes the transfer through the scales of the mean turbulent temperature (or velocity) energy. For simplicity, Eq. (3) will be written as: $A+B=C$, where A is the turbulent transport term, B is the dissipative term, and C is the linear term [note that A, B and C are respectively equivalent to I, III and II in the PDF Eq. (2)]. Figure 9 presents the verification of Yaglom's equation, where dimensionless scales have been used, in the manner that: $C = \frac{4}{3} r / \eta$. Similar results are obtained when verifying Eq. (4).

Studying the relative balance between the three terms, the temperature dissipative range is defined as being for scales smaller than 20η , whereas the temperature inertial range is that for scales larger than 40η .

As seen in Sec. III A, the dynamical inertial range was defined using classical criteria and it extends from 20η to 150η . The temperature inertial range is slightly displaced towards larger scales. This is a typical behavior for a mixing where velocity and temperature have different injection scales. In this inertial range and for this rather large R_λ

$= 600$, Yaglom's equation is verified over the entire inertial range: $A+B=C$, as it can be verified in Fig. 9. Yaglom's equation verification is a necessary step towards Eq. (2) verification, and moreover it provides an indication about the range of scales where this verification can be expected to be valid. It is also a good indicator about the turbulent mixing level. For relatively high Reynolds numbers, as it is the case here, the turbulent transport term $\langle \Delta u (\Delta \theta)^2 \rangle$ equilibrates well the total dissipation. On the other hand, since intermittency effects are not seen via Eq. (4), higher level statistics need to be investigated in order to study intermittency. From this point of view, the PDF evolution through the scales gives a complete information about the intermittency effects on the cascade. Yaglom's equation represents a "folded map" where the intermittency information is compressed and reduced at the second order level.

C. Integration of the PDF equation

Using the two conditional expectations q_1 and q_2 (in Fig. 8) and an initial condition at 80η (the PDF and the derivative at this scale), we then integrate numerically Eq. (2). Details about our numerical method may be found in Ref. 12. The numerical integration is carried out using a finite differences scheme, and a negative scale r step $\delta r = -0.001$, in order to respect the numerical scheme stability and precision criteria. Starting from a large scale PDF, the equation solution is computed for the smaller scales.

The numerical solution is quite sensitive to the initial condition (PDF and its derivative), and it is therefore sensitive to the choice of this initial integration scale. This behavior is strictly correlated with the equation verification, i.e., the computation of the three terms appearing in Eq. (2), written as $I+II=III$. As observed,¹² term III is present only for very small scales, where molecular dissipation is the relevant phenomenon. For intermediate scales ($r \geq 10\eta$), $III \approx 0$, and the balance equation is thus reduced to $I = -II$. Here, both terms are well balanced for the scales smaller than 80η . For much larger scales, the turbulent transport term I is negligible, and term II , expressed through a "diffusion in the X space," which is classical of PDF models,³⁶ remains unbalanced (just as the linear term C , its counterpart in Yaglom's equation, remains unbalanced at large scales). The evolution equation is not verified for these large scales since a large scale "source term" would be required to describe the way turbulent energy is fed into the cascade. Discussing in more detail this specific problem is clearly not the objective of the present work. Figure 10 illustrates this balance between terms I and II ($I = -II$) at 80η , and the breakdown of this equilibrium for $r = 200\eta$, where $I \ll II$.

In this light, the numerical treatment will involve two steps, the first one consisting in finding an initial condition which is solution of Eq. (2). The upper limit of the validation domain is defined as the scale (80η), where Eq. (2) is verified with a 10% accuracy. Starting from this scale, the computed solution possesses the real physical aspect, and the numerical solution better and better verifies the equation through the small scales.

Note that, in previous studies,¹² this limit was only 40η ,

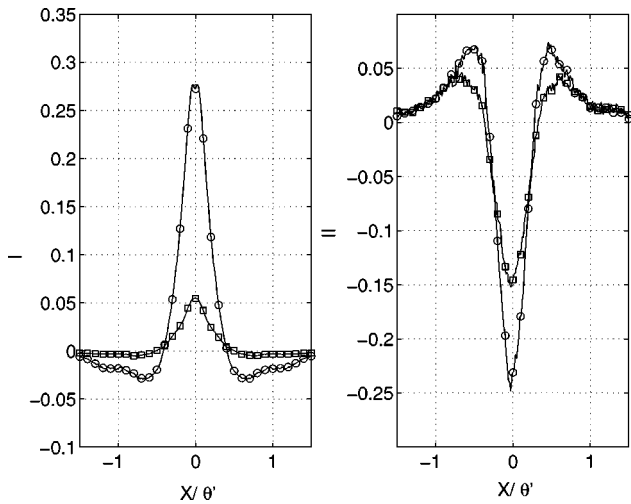


FIG. 10. Vaienti *et al.* equation verification: the terms *I* (left) and *II* (right) are well balanced at 80η (\circ), and are not balanced at 200η (\square), where $II \gg I$.

so that our present success is a substantial progress in understanding the PDF evolution through the scales.

The second step of our approach is the calculation, through Eq. (2), of the PDF evolution. Figure 11 shows the numerical solutions for the scales $80\eta, 60\eta, 30\eta, 15\eta$ and 5η (solid line and symbols) which compare favorably well with the real PDFs (dotted line). Let us remark in particular that the PDF exponential tails³⁷ are well predicted (note the logarithmic vertical scale).

In fact, the computed PDFs are in very good agreement with the real PDFs, apart from the slightly asymmetric features which obviously cannot be obtained when solving the PDF evolution equation, for the scales $80\eta, 60\eta, 30\eta$ and 15η down to probability levels of about 10^{-2} . Such a good level of agreement is worth noticing if one considers the q_1 oscillations which were previously discussed. Much longer measurement time would be necessary in order to achieve

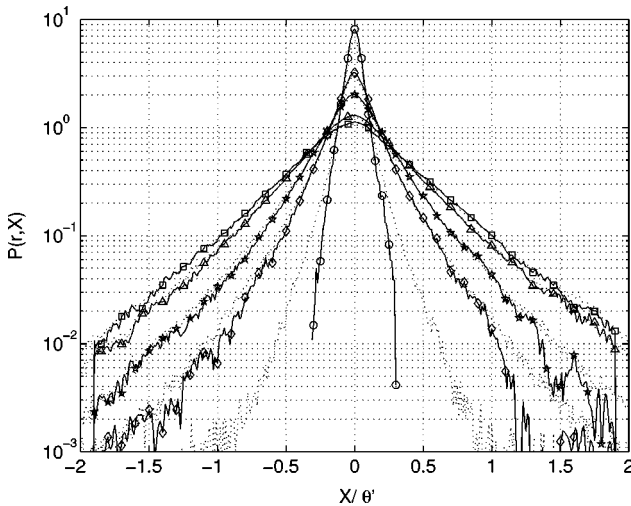


FIG. 11. Numerical solution of 2, for the scales 80η (\square), 60η (\triangle), 30η (\star), 15η (\diamond) and 5η (\circ), compared to the real PDFs (dotted lines).

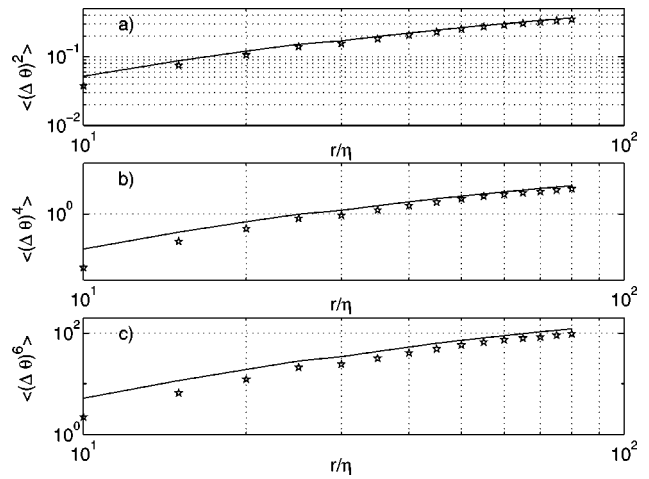


FIG. 12. Comparison between real moments (solid lines) and simulated moments (\star): second order (a), fourth order (b), and sixth order (c).

more precise closures for large fluctuations of temperature increments.

In order to further validate our results, the real moments have been computed, up to order 6, and are compared with the “simulated” moments, i.e., those obtained using the numerical solution of 2. Results are presented in Fig. 12, for the range of scales $[10\eta - 80\eta]$. A good agreement is obtained, especially near the “initial condition,” here the scale 80η . To compare quantitatively the true and the simulated moments, we compute the scaling exponents. These are obtained by the optimum compensation of the structure functions. Thus, the real ones are inferred from the range $[40\eta, 150\eta]$, and the “simulated” ones present a plateau between $[50\eta, 80\eta]$.

The real scaling exponents are: $\zeta_4 = 1$ and $\zeta_6 = 1.15$, and can be compared with $\zeta_{4\text{sim}} = 1.05$ and $\zeta_{6\text{sim}} = 1.2$, obtained from the numerical solution of Eq. (2). The computed exponent is slightly larger than the real one, signifying in a way less intermittency.

Starting from 80η as the initial condition, the smaller scale PDFs, or corresponding moments are fairly well-predicted using Eq. (2), and the measured conditional expectations. In particular, the PDF intermittent behavior is obtained with relatively high accuracy. As already emphasized,¹² the studied approach is always verified for the small scales. The upper verification limit depends on the Pe number of the mixing. Here, the large Pe number, and the symmetry of the mixing, permitted us to validate it in a large part of the inertial zone. Note here that this validation limit (80η) is situated in the central part of the inertial zone. Supplementary, Eq. (2) does not admit as the initial condition PDFs measured at scales larger than 80η . The initial condition PDF is not Gaussian, and it depends on the large injection scales, in another manner implicating the injection modality and the particular geometry of the flow. Also, both conditional expectations contain information about the large scale phenomena. For understanding how small scale conditional expectations are influenced by the large scale anisotropy, more efforts are required in order to obtain a theoretical expression for the closures, in different kinds of mixings.

This objective is, here again, quite beyond the scope of the present work.

Thus, further work should investigate how the input data of the approach (initial condition and closures) inherit and transmit through the scale evolution some particular characteristics of each mixing flow, such as the large-scale injection manner and asymmetries. More studies are presently performed in order to understand the link between the large scales and the small scales.

V. CONCLUSION

The mixing in the counter-rotating Von Kármán swirling flow has been analyzed. This experimental set-up presents various advantages: a large turbulent Reynolds number in a small space volume, a central region where the dynamic field is almost homogeneous and isotropic, and a double temperature source (cold and hot) used as an original means to create some interesting properties of the mixing.

Thus, it was possible to create in the central part of the flow a region where two isotropic criteria are reasonably well respected: a null velocity-temperature correlation coefficient and a small temperature increment skewness factor. In particular, the temperature derivative skewness factor can be as small as 0.01, contrary to the value usually met in a single-source mean temperature gradient mixing where its absolute value is classically about 0.8. These better isotropic conditions, and the large Pe number of the mixing ($Pe \approx 400$), permitted us to successfully integrate numerically the Vaienti *et al.* Eq. (2) for a scale range extending on a large part of the inertial zone (up to 80η), and to predict with reasonable accuracy the intermittent behavior of the PDFs. The integration needed no symmetrization for the PDFs and the two incoming closures, as it is necessary in a boundary layer or in a jet. Even though efforts must now be devoted to obtain with more precision the q_1 evolution through the scales and the influence of the large scale properties on small scale statistics, the present results demonstrate that this Eq. (2) is a real powerful tool to study the passive scalar small-scale intermittency effects. Additional studies are presently performed in order to take explicitly into account the temperature mean gradient role, to understand in this manner the large-scale PDF evolution, and to derive the expression of the large-scale term which must be incorporated into Yaglom's (and also Kolmogorov's) equation as well as into the PDF equation.

ACKNOWLEDGMENTS

We acknowledge the support of DRET, under Contract No. 95/2592A,B and C. The authors thank R. A. Antonia, J. Dušek, and A. Pumir for fruitful discussions.

¹A. S. Monin and A. M. Yaglom, *Statistical Fluid Mechanics* (MIT Press, Cambridge, 1975), Vol. 2.

²F. Anselmet, Y. Gagne, E. J. Hopfinger, and R. A. Antonia, "High-order velocity structure functions in turbulent shear-flows," *J. Fluid Mech.* **140**, 163 (1984).

³S. Corrsin, "On the spectrum of isotropic temperature fluctuations in iso-

tropic turbulence," *J. Appl. Phys.* **22**, 469 (1951); A. M. Oboukhov, "Structure of the temperature field in turbulent flows," *Izv. Akad. Nauk SSSR Geogr. Geofiz.* **13**, 58 (1949).

⁴R. A. Antonia, E. J. Hopfinger, Y. Gagne, and F. Anselmet, "Temperature structure functions in turbulent shear flows," *Phys. Rev. A* **30**, 5 (1984).

⁵C. Meneveau, K. R. Sreenivasan, P. Kailasnath, and M. S. Fan, "Joint multifractal measures: Theory and applications to turbulence," *Phys. Rev. A* **41**, 894 (1990).

⁶E. Lévêque, S. Ciliberto, C. Baudet, and G. Ruiz-Chavarría, "Statistical properties of the energy flow of a passive scalar in fully developed turbulence," *Advances in Turbulence VII*, edited by U. Frisch (Kluwer Academic, New York, 1998).

⁷G. He and B. Dubrulle, "About generalized scaling for passive scalars in fully developed turbulence," *J. Phys. II* **7**, 793 (1997).

⁸R. H. Kraichnan, "Anomalous scaling of a randomly advected passive scalar," *Phys. Rev. Lett.* **78**, 4922 (1997), and references therein.

⁹E. Ching, V. S. L'vov, and I. Procaccia, "Fusion rules and conditional statistics in turbulent advection," *Phys. Rev. E* **54**, 4520 (1996).

¹⁰S. Vaienti, M. Ould-Rouis, F. Anselmet, and P. Le Gal, "Statistics of temperature increments in fully developed turbulence: Part 1: Theory," *Physica D* **73**, 99 (1994).

¹¹M. Ould-Rouis, F. Anselmet, P. Le Gal, and S. Vaienti, "Statistics of temperature increments in fully developed turbulence: Part 2: Experiments," *Physica D* **85**, 405 (1995).

¹²L. Danaila, F. Anselmet, P. Le Gal, J. Dusek, C. Brun, and A. Pumir, "Predictions of small-scale statistics for a passive scalar in turbulent mixing," *Phys. Rev. Lett.* **79**, 4577 (1997).

¹³R. A. Antonia and C. W. Van Atta, "Structure functions of temperature fluctuations in turbulent shear flows," *J. Fluid Mech.* **84**, 561 (1978).

¹⁴P. Mestayer, "Local isotropy and anisotropy in a high-Reynolds-number turbulent boundary layer," *J. Fluid Mech.* **125**, 475 (1982).

¹⁵K. R. Sreenivasan, "On local isotropy of passive scalars in turbulent shear flows," *Proc. R. Soc. London, Ser. A* **434**, 165 (1991).

¹⁶M. Holzer and E. D. Siggia, "Turbulent mixing of a passive scalar," *Phys. Fluids* **6**, 1820 (1994).

¹⁷A. Pumir, "A numerical study of the mixing of the passive scalar in three dimensions in the presence of a mean gradient," *Phys. Fluids* **6**, 2118 (1994).

¹⁸C. Tong and Z. Warhaft, "On passive scalar derivative statistics in grid turbulence," *Phys. Fluids* **6**, 2165 (1994).

¹⁹C. Bégulier, L. Fulachier, and J. F. Keffer, "The turbulent mixing layer with an asymmetrical distribution of temperature," *J. Fluid Mech.* **89**, 561 (1978).

²⁰K. R. Sreenivasan, S. Tavoularis, and S. Corrsin, "A test of gradient transport and its generalizations," in *Turbulent Shear Flows 3*, edited by L. J. S. Bradbury, F. Durst, B. E. Launder, F. W. Schmidt, and J. H. Whitelaw (Springer, Berlin, 1981), p. 96.

²¹J. Maurer, P. Tabeling, and G. Zocchi, "Statistics of turbulence between two counter-rotating disks in low-temperature helium gas," *Europhys. Lett.* **26**, 31 (1994).

²²J. F. Pinton and R. Labbé, "Correction to the Taylor hypothesis in swirling flows," *J. Phys. II* **4**, 1461 (1994).

²³J. F. Pinton, F. Plaza, L. Danaila, P. Le Gal, and F. Anselmet, "On velocity and passive scalar scaling laws in a turbulent swirling flow," *Physica D* **122**, 187 (1998).

²⁴L. W. B. Browne and R. A. Antonia, "The effect of wire length on temperature statistics in a turbulent wake," *Exp. Fluids* **5**, 426 (1987).

²⁵J. C. Wyngaard, "Spatial resolution of a resistance wire temperature sensor," *Phys. Fluids* **14**, 2052 (1971).

²⁶L. Fulachier, "Hot wire measurements in low speed heated flow," in *Proceedings of the Dynamic Flow Conference* (P.O. Box 121, DK-2740, Skovlunde, Denmark, 1978).

²⁷R. Chevray and N. K. Tutu, "Simultaneous measurements of temperature and velocity in heated flow," *Rev. Sci. Instrum.* **43**, 1417 (1972).

²⁸G. K. Batchelor, *The Theory of Homogeneous Turbulence* (Cambridge University Press, Cambridge, 1953).

²⁹A. Pumir, "Small scale properties of scalar and velocity differences in three-dimensional turbulence," *Phys. Fluids* **6**, 3974 (1994).

³⁰L. Mydlarski and Z. Warhaft, "Passive scalar statistics in high-Péclet-number grid turbulence," *J. Fluid Mech.* **358**, 135 (1998).

³¹K. R. Sreenivasan and S. Tavoularis, "On the skewness of the temperature derivative in turbulent flows," *J. Fluid Mech.* **101**, 783 (1980).

³²R. A. Antonia, A. J. Chambers, C. W. Van Atta, C. A. Friehe, and K. N.

- Helland, "Skewness of temperature derivative in a heated grid flow," *Phys. Fluids* **21**, 509 (1978).
- ³³K. R. Sreenivasan, R. A. Antonia, and D. Britz, "Local isotropy and large structures in a heated turbulent jet," *J. Fluid Mech.* **94**, 745 (1979).
- ³⁴R. A. Antonia, F. Anselmet, and A. J. Chambers, "Assessment of local isotropy using measurements in a turbulent plane jet," *J. Fluid Mech.* **163**, 365 (1986).
- ³⁵A. M. Yaglom, "On the local structure of a temperature field in a turbulent flow," *Dokl. Akad. Nauk SSSR* **69**, 743 (1949).
- ³⁶E. E. O'Brien, "The probability density function (PDF) approach to reacting turbulent flows," in *Turbulent Reacting Flows*, edited by P. A. Libby and F. A. Williams (Springer, Berlin, 1980), Vol. 44.
- ³⁷E. S. C. Ching, "Probabilities for temperature differences in Rayleigh-Bénard convection," *Phys. Rev. A* **44**, 3622 (1991).